ACS APPLIED MATERIALS & INTERFACES

Letter

www.acsami.org

ZnO Nanowire-Based Antireflective Coatings with Double-Nanotextured Surfaces

Jae Won Lee,[†] Byeong Uk Ye,[†] Dong-yeong Kim,[‡] Jong Kyu Kim,[‡] Jong Heo,[‡] Hu Young Jeong,[§] Myung Hwa Kim,[⊥] Won Jun Choi,[#] and Jeong Min Baik*,[†]

[†]School of Mechanical and Advanced Materials Engineering, KIST-UNIST-Ulsan Center for Convergent Materials, Ulsan National Institute of Science and Technology (UNIST), Ulsan, 689-798, Korea

[‡]Department of Materials Science and Engineering, Pohang University of Science and Technology (POSTECH), Pohang, Gyungbuk 790-784, Korea

[§]UNIST Central Research Facilities (UCRF), Ulsan National Institute of Science and Technology (UNIST), Ulsan, 689-798, Korea

[⊥]Department of Chemistry & Nano Science, Ewha Womans University, Seoul 120-750, Korea

[#]Nano-Photonics Center, Korea Institute of Science and Technology, Seoul 136-791, Korea

ABSTRACT: High-aspect-ratio nanotextured surfaces with different morphologies (straight, core−shell type, and core−branch type nanowires) are prepared by a hydrothermal method of ZnO nanowires, followed by means of RF sputtering for core−shell type nanowires and e-beam evaporation for branch-type nanowires. The structural analysis showed that the MgO has highly preferred orientation along the ⟨111⟩ and ⟨200⟩ direction, respectively, and the crystalline continuity between the ZnO and MgO layers were also showed. Compared with ZnO nanowires, the MgO/ZnO samples drastically suppress broad and omnidirection reflection, which ascribes to the refractive-index modulation along the lateral direction of nanowires growth as well as the vertical direction. It was also shown that morphology could have a substantial influence on the antireflection property. These results suggest that double-nanotextured surface is one of the promising structures for antireflective surfaces without fine control in nanowire morphology.

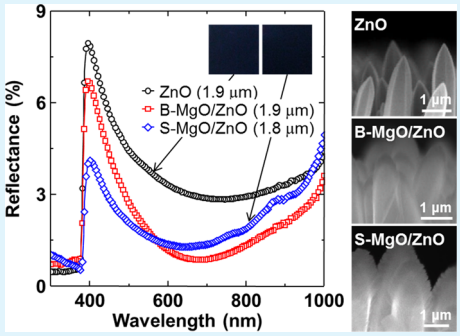

KEYWORDS: *antireflection, AR coating, ZnO nanowire, core−shell, core−branch, MgO*

INTRODUCTION

One-dimensional (1D) nanostructures of metal oxide semiconductors such as ZnO, have currently attracted great attention due to their potential applications in fabricating electronic, optoelectronic, electromechanical, and electrochemical devices, such as solar cell,[1] light-emitting diodes,[2] sensor,[3] ultraviolet laser,[4] and nanogenerator.[5] In particular, morphology-dependent physical and optical properties of 1D nanostructures with stable and controlled size and shape have been widely studied with the objective of enhancing the performance of the above devices.

Antireflective (AR) surfaces based the 1D ZnO nanostructures may be one of promising applications due to the subwavelength structure, wide bandgap, and excellent optical properties of ZnO, although there are a variety of AR coatings, such as nanostructures by oblique incidence deposition,[1,6] replicated polymer structures,[7] tailored silicon surfaces,[8] etched fused silica and glass surfaces,[9] carbon nanotube arrays,[10] and nanoporous polymers.[11] Lee et al. reported that an efficient AR coating using ZnO nanorods with the weighted reflectance of 6.6% at the wavelengths ranging from 400 to 1200 nm could enhance solar cell performance by nanoscale tuning of surface morphology such as the thickness of ZnO seed layer and tapering of nanorod tips.[12,13] Atomically sharp nanorod taper may be one of promising approaches for AR surfaces because the refractive index is dependent on the volume fraction of the AR structure, Actually, Yeh et al. showed that the AR layers based on the ZnO nanorod arrays terminated with ultrasharp tips were successfully fabricated and could improve the external quantum efficiency from 14.5 to 19.1%.[12] The ZnO nanorods with large alignment variation such as flowerlike morphology also showed broadband and omnidirectional low reflection.[14] Thus, most work has focused on the fine control of morphologies in ZnO nanowires; however, it may not be easy to obtain favorable tip geometry to obtain a smooth graded refractive-index because there are so many influencing factors in growing the nanowires such as substrate, amount of precursor, growth time, temperature, additives, etc.[12,15]

In present day, a series of hierarchical MgO/ZnO-based nanostructures with different and controlled morphologies (core−shell type and core−branch type) are simultaneously examined within the same test apparatus, enabling lower reflection over a wide angle and a broad wavelength without fine growth controls in ZnO nanowires itself, compared with

Received: November 20, 2013
Accepted: January 27, 2014
Published: January 27, 2014

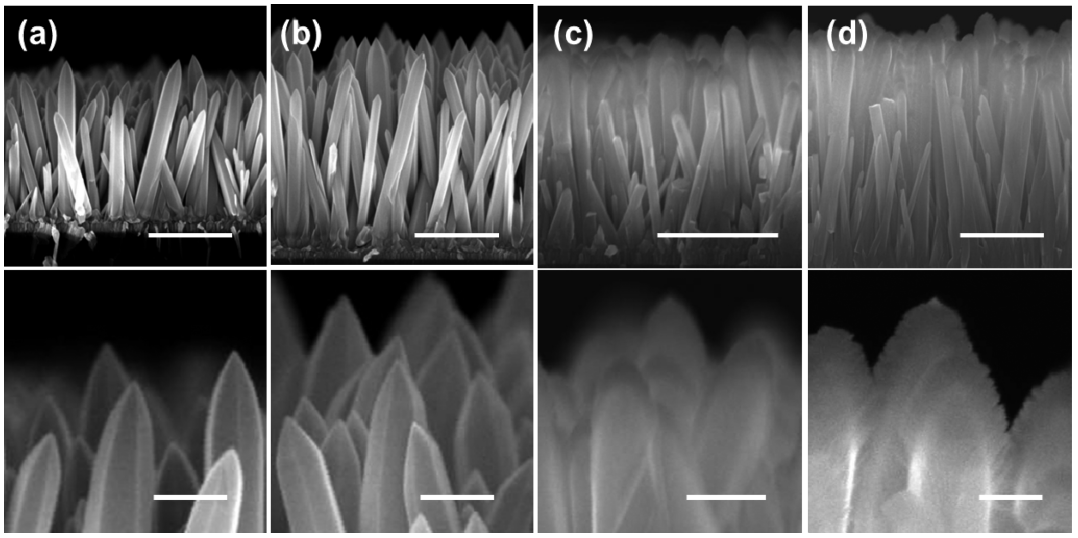

Figure 1. SEM images of (a, b) ZnO nanowire arrays with different length, (c) MgO/ZnO core−shell nanowires, and (d) MgO/ZnO core−branch nanowires. The scale bars are 1 μm and 200 nm, respectively.

the pristine ZnO nanowires. It is believed that the total reflection of the light with a low angle of incidence can be significantly lowered by refractive-index modulation along the lateral direction of nanowires growth as well as the vertical direction, supported by finite element simulation using COMSOL multiphysics.

EXPERIMENTAL SECTION

High-aspect-ratio MgO/ZnO double-nanotextured surfaces with core−shell and core−branch morphologies were prepared via a hydrothermal method of ZnO nanowires, followed by means of RF sputtering for core−shell nanowires and e-beam evaporation for branch-type nanowires, respectively. An approximately 100 nm layer of ZnO, which acts effectively as the seed layer for growing ZnO nanowires, is deposited by reactive sputtering using 100 W of RF power to the 2 in. ZnO target, 16 SCCM (SCCM denotes cubic centimeter per minute at STP) of Ar and 4 SCCM of O_2 at an operating pressure of 4 mTorr. For the nanowires synthesis, a well-known method, the growth solution for hydrothermal preparation of ZnO was prepared by mixing 0.025 M zinc nitrate hydrate and 0.025 M hexamethylenetetramine (HMT) in DI water. The MgO/ZnO core−shell nanowires were fabricated using 100 W of RF power to the 2 in. MgO target, 16 SCCM of Ar and 4 SCCM of O_2 at an operating pressure of 4 mTorr. MgO/ZnO core−branch nanowires were prepared by e-beam evaporation using high purity MgO pellet (99.99% with a diameter of 3 mm). The MgO layer was grown at a rate of 0.5 nm/s at room temperature. The samples are then annealed at 400 °C to enhance the crystalline properties.

The total reflectance spectra of the nanowires on Si substrate were measured at an unpacked (on-wafer) configuration using an integrating sphere. The scanning electron microscopy (SEM) was done using a PHILIPS XL30S with an accelerating voltage of 10 kV. The high-resolution transmission electron microscopy (HR-TEM) images were collected using a Cs-corrected JEM-2100 operated at 200 kV. Reflectance data were obtained at wavelengths ranging between 300 and 1000 nm using a UV−vis spectrometer (Perkin-Elmer Lambda 750) equipped with integrating sphere. The reflected light is collected into the angular acceptance range characterized by the minimum and maximum acceptance angles. To verify the effect of MgO on reflectance, we employed COMSOL multiphysics software with a RF module for two-dimensional finite element frequency domain simulation.

RESULTS AND DISCUSSION

Figure 1 shows SEM images of typical nanowire arrays: pristine ZnO nanowires (a, b), ZnO nanowires with straight MgO shells (c), and ZnO nanowires with nanobranched MgO shells (d). The ZnO nanowires seen in images a and b in Figure 1 are approximately 1.8−1.9 and 2.7−2.8 μm long, respectively, by tuning the growth time, whereas the nanowire diameter of both samples is in the range of 180 nm, with similar diameter distributions. The nanowires in both samples show similar tapered shapes with approximately 200 nm in length and 60° in angle from the top of the nanowires. Thus, one may observe the effects of the length of the nanowires on the reflectance, by excluding the effects of the tapered shape. By using RF magnetron sputtering, MgO films were deposited on the ZnO nanowires and core−shell nanowires with straight MgO shells of approximately 20−30 nm at the sidewall and 70−80 nm at the top were formed. On the contrary, the MgO deposition by an e-beam evaporator produced the branch type shells having a diameter less than 20 nm and a length of 100−120 nm at the top. Although the physical deposition method may not allow the formation of uniform MgO shells, they appear to be tight and uniform along the body of the nanowires up to 100−200 nm.

The crystal structures of MgO layers and at the interface of MgO and ZnO layers were characterized by high-resolution TEM images. Figure 2a, c, and e show high-resolution SEM image and TEM images with the fast Fourier transform (FFT) of a core−shell type nanostructure. Thin MgO shells are clearly visible, and they appear to be tight and quite uniform along the body of the nanowires although it is seen that the MgO layer at the tip is thicker. When very thin (~5 nm) MgO layer was formed (Figure 2c), the corresponding atomic spots and the diffraction pattern reveal highly ordered lattices, implying highly crystalline properties of the MgO layer. FFT patterns taken along the $[1\bar{2}10]$ zone axis, together with measured lattice spacing of the adjacent planes, confirm that c-axial ZnO

dx.doi.org/10.1021/am4051734 | ACS Appl. Mater. Interfaces 2014, 6, 1375−1379

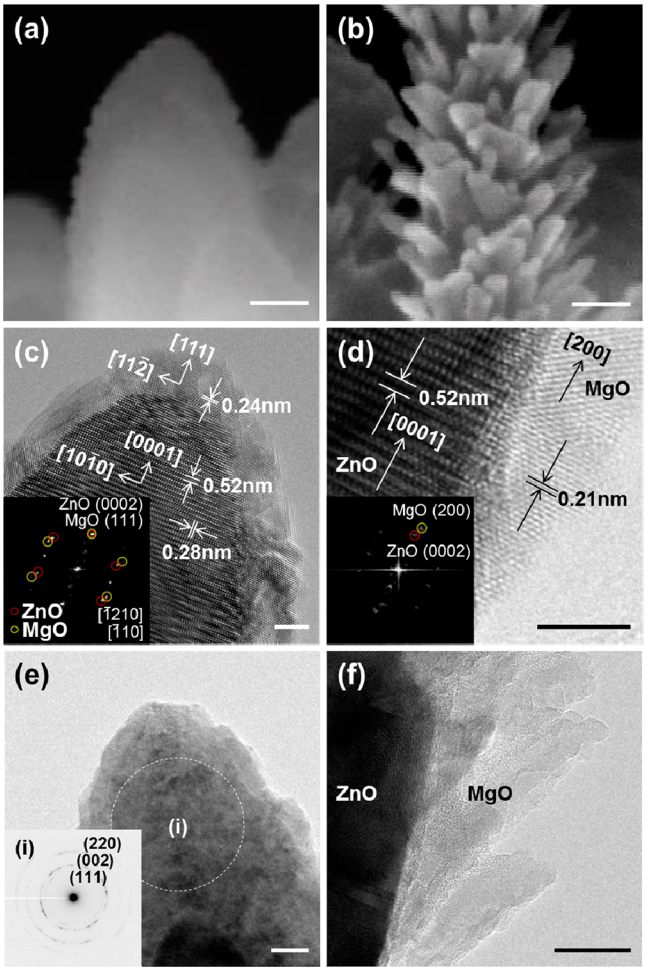

Figure 2. (a, b) High-resolution SEM images and (c–f) TEM images of MgO/ZnO core–shell nanowires and MgO/ZnO core–branch nanowires. Five and one-hundred nanometer thick MgO were deposited on the ZnO surface in c, d and e, f, respectively. Scale bars: (a, b) 100, (c, d) 5, and (e, f) 20 nm.

nanowires have (10$\bar{1}$0) side planes. High magnification at the interface region clearly shows well-matched structure between the [11$\bar{2}$] basal plane of MgO (111) and [10$\bar{1}$0] basal plane of ZnO (0002), demonstrating the crystalline continuity between two materials, reported previously.[16,17] Further increase in the MgO thickness (100 nm) produces the core–shell type nanostructure (Figure 2a) and the corresponding diffraction pattern reveals that the MgO layer is poly crystalline. Figure 2b, d, and f shows a high-resolution SEM image and TEM images with the FFT of a branch-type nanostructure. Before the growth of the MgO nanobranches, a very thin (5–7 nm) MgO layer is formed on the surface. Figure 2d shows a high-resolution TEM image taken from the interface area of ZnO and MgO. The regular atom arrangement is displayed at the interface region also shows the crystalline continuity between the ZnO and the MgO layer. As the thickness of the MgO layer increases, MgO nanowires are clearly visible, grew to about 20 nm in diameter. On the top of the ZnO nanowires, it is seen as a form of fan shape consisting of many nanowires. These aspects, which are currently being investigated, will be the subject of a separate publication.

To investigate the AR characteristics of hierarchical MgO/ZnO-based nanostructures over the broad range of wavelengths, we observed the total reflection over a wavelength range from 300 to 1000 nm, as shown in Figure 3a. The incident angle with respect to the parallel of the sample was 82

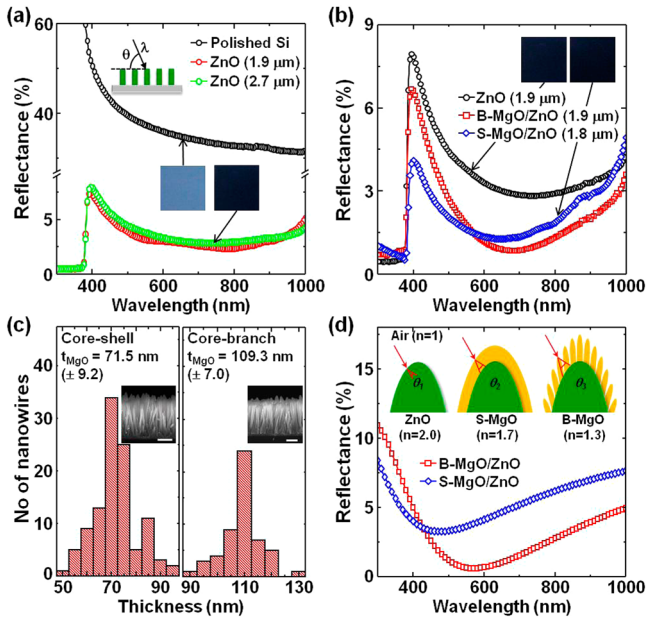

Figure 3. Total reflection spectra over a wavelength range from 300 to 1000 nm: (a) polished Si substrate and ZnO nanowires on the Si; (b) ZnO nanowires, MgO/ZnO core–shell, and MgO/ZnO core-branch nanowires. (c) Histogram of the size distributions of MgO for MgO/ZnO core–shell and MgO/ZnO core–branch. The insets are the SEM images of MgO/ZnO core–shell nanowires and MgO/ZnO core-branch nanowires. (the scale bar is 1 um). (d) Reflectance curve predicted by CMT is given for MgO/ZnO core–shell and MgO/ZnO core–branch nanowires. The insets are the schematic diagrams of the light path entering ZnO, straight MgO, branch MgO.

° in this measurement. Over this measured range, the polished Si substrate is shown to reflect over 30% of the incident light and the reflectance is increased up to over 60% as the wavelength is reduced to 300 nm. After growing the ZnO nanowires with a thickness of 1.9 μm on Si substrate, the reflectance is reduced over a broad wavelength range to around 5% or less over a wavelength range from 500 to 1000 nm, well-known and usually attributed to the decrease in effective refractive index along the body of the nanowires from the bottom due to the tip geometry. However, it still shows high reflectance (5–8%) at lower wavelength than 500 nm. A further increase in the length of the nanowires to 2.8 μm, obtained by increasing the growth time, does not affect the performance of the antireflective surfaces. Actually, even if the growth time increases, there is no significant change in the tapering angle toward the tip and the length of tapered region. This fact might imply no significant effects of length of the nanowires longer than critical length (~2 μm) on the antireflection properties.[18]

There has been long interest in fine control in nanowire tip diameter for the applications such as field-emission devices,[15] light-emitting diodes,[19] photodetectors,[20] near-field microscopy, as well as AR coatings. The additives such as 1,3-diaminopropane and Al ions into the growth solution promoted the growth of high-aspect-ratio nanowires by prohibiting the lateral growth of the nanowires.[21,22] Fine control in the growth temperature can also create highly tapered nanowires.[23,24] However, there are so many influencing factors in growing the nanowires such as substrate, amount of

dx.doi.org/10.1021/am4051734 | ACS Appl. Mater. Interfaces 2014, 6, 1375–1379

precursor, growth time etc., other than temperature and additives.[25] These will make it difficult to control the growth precisely.

In the mean time, nanometer-size or nanostructured low-refractive-index materials such as SiO_2, MgO, and MgF_2 on the surface of ZnO nanowires may reduce the reflectance without fine control in the tip geometry of the nanowires and may be suggested to be an alternative method for the antireflective surface. As expected and in accordance to the above refractive index adjustment, the straight MgO shell on the surface of ZnO nanowires further reduced the reflectance in the range of 400 to 1000 nm (Figure 3b). Note that as the wavelength decreases, the further decrease in the reflectance is observed. At the wavelength of 400 nm, the reflectance is reduced nearly twice up to 4%. The branch-type MgO layer also shows lower reflectance than that of pristine ZnO nanowires, but poor reflectance compared with the core−shell type nanostructures. According to the effective medium approximation,[26,27] the effective refractive index is calculated to be 1.3, smaller than that (~1.7) of MgO film, by assuming that the porosity of MgO nanobranches is about $P = 75\%$. This implies that the gradient of the refractive index is less abrupt in branch-type nanostructures. This will make the angle of the refracted light in branch-type nanostructures increase by Snell's law, resulting in a lower reflectance than that of the core−shell type nanostructures and dark appearance in the spectral range. The reflectance was simulated by characteristic matrix theory and was given by[28]

$$R = \frac{(n_0 - n_{ZnO})^2 \cos^2\frac{\delta}{2} + \left(\frac{n_0 n_{ZnO}}{n_{MgO}} - n_{MgO}\right)^2 \sin^2\frac{\delta}{2}}{(n_0 + n_{ZnO})^2 \cos^2\frac{\delta}{2} + \left(\frac{n_0 n_{ZnO}}{n_{MgO}} + n_{MgO}\right)^2 \sin^2\frac{\delta}{2}}$$

where R is the reflectance of an incident light, n_0, n_{ZnO}, and n_{MgO} are the refractive indices of the air, ZnO, and MgO. δ is the phase angle given by $4\pi n_{MgO} h/\lambda \cos(90 - \theta)$, in which h is the thickness of MgO and θ is the incident angle of light. The thicknesses for the straight MgO and branch MgO characterized by the CMT are 70 and 110 nm (Figure 3c), respectively. Assuming the light is incident on the top of the nanowires ($\theta = 90°$), it is clearly observed that the core−shell type nanostructures show lower reflectance than that of the branch-type nanostructures at low wavelength. As the wavelength increases, the branch-type nanostructures show lower reflectance, consistent with the experimental results, as shown in Figure 3d.

To investigate the effect of the straight MgO shell on the omnidirectionality of the antireflective surface, we measured the total reflection of the straight MgO shells at low angles (20 and 30°) with the surface over a wavelength range from 300 to 1000 nm, plotted in Figure 4. As the angle of incidence decreases to 20°, the reflectance of all samples with only ZnO nanowires significantly increases up to 20% at 400 nm. As the light reaches the surface at a low angle, less light enters the nanowire layers and thus light trapping within the layers is reduced, leading to an increase in reflectance. By forming MgO shells on the surface of ZnO nanowires, the reflectance is reduced the reflectance over a broad wavelength AR layers. At 400 nm, the reflectance is reduced from 20.6 to 15.1% and 10.8 to 7.4% at an angle of 20 and 30°, respectively. Thus, the surface of ZnO nanostructure and hierarchy may be advantageous for omnidirectional antireflective surface.

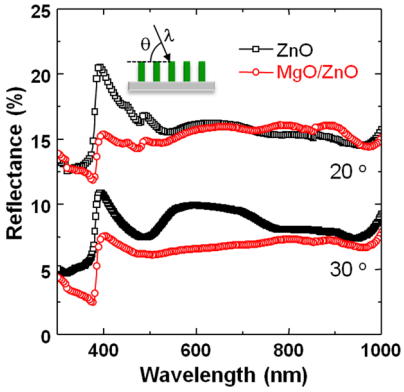

Figure 4. Total reflectance with the angle of incidence of 20 and 30° for ZnO nanowires array on Si and MgO/ZnO core−shell nanowires over a wavelength range from 300 to 1000 nm.

To verify the effect of the straight MgO shell on the reflectance, we performed finite element simulation using COMSOL multiphysics. The simulated structure was composed of 200 nm thick Si layer, 100 nm thick ZnO seed layer, and 2 μm height tapered ZnO nanowires coated by 20 nm thick MgO shells, in which the ZnO diameter is about 200 nm at the bottom and is gradually decreased along the body of the nanowires to 150 nm, as shown in the SEM images (Figure 1). ZnO nanowire arrays were realized by periodic boundary condition. In addition, perfect matched layer covered by scattering boundary condition was imposed on the underside of the Si layer to ensure that the Si layer completely absorbs the incident light. Extinction coefficients of both ZnO and MgO were set to zero in order to focus on the effect of refractive index modulation on the reflectance. Electromagnetic wave came into the structure through the top side.

Figure 5a shows wavelength dependence of reflectance at normal incident ($\theta = 90°$). Reflectance of polished Si from the finite element simulation matches both the calculated reflectance based on the Fresnel's equation and experimentally

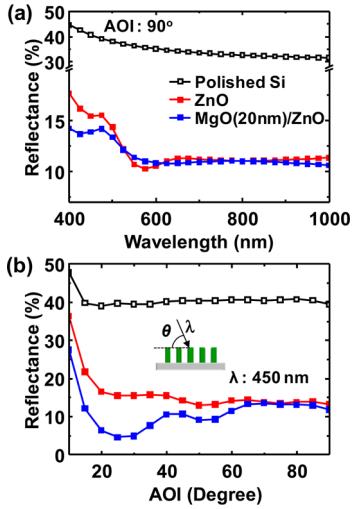

Figure 5. COMSOL multiphysics software with RF module was employed for two-dimensional finite element frequency domain simulation. (a) Wavelength-dependent simulated reflectance distribution at 90°, (b) AOI-dependent simulated reflectance distribution at 450 nm of polished Si, ZnO NWA, 20 nm thickness S-MgO/ZnO NWA.

measured one. ZnO nanowires on Si substrate significantly reduce the reflectance to around 12% or less over a broad wavelength range of 530 to 1000 nm. However, it still shows high reflectance (>15%) at a shorter wavelength than 530 nm. Reflectance in this regime can be decreased by forming MgO shells on the ZnO nanowires. More interestingly, reflectance is significantly decreased at low angles (20−35°) of light incidence by forming the MgO shells on the ZnO nanowires (Figure 5b). This simulation result implies that the decrease in reflection is attributed to the effect of the refractive index gradient enabled by the MgO shells that increases especially at the low incident angles.

CONCLUSIONS

In summary, we demonstrated that high-aspect-ratio double-nanotextured surfaces with different morphology such as core−shell type and core-branch type nanowires were one of promising structures for antireflective surfaces without fine control in nanowire morphology. The core−shell and core−branch nanowires were prepared by RF sputtering and e-beam evaporation of MgO, respectively. The structural analysis showed that the MgO has highly preferred orientation along the ⟨111⟩ and ⟨200⟩ direction, respectively, and the crystalline continuity between the ZnO and MgO layers were also showed. Compared with ZnO nanowires, the MgO/ZnO samples drastically suppress broad and omnidirection reflection, which ascribes to the refractive-index modulation along the lateral direction of nanowires growth as well as the vertical direction, supported by finite element domain simulation.

AUTHOR INFORMATION

Corresponding Author

*E-mail: jmbaik97@gmail.com.

Notes

The authors declare no competing financial interest.

ACKNOWLEDGMENTS

This research was supported by the Converging Research Center Program through the Ministry of Science, ICT and Future Planning, Korea (2013K000196), by the Pioneer Research Center Program through the National Research Foundation of Korea funded by the Ministry of Science, ICT & Future Planning (NRF-2013M3C1A3063602), and by the Future Strategic Fund (1.130061.01) of UNIST (Ulsan National Institute of Science and Technology).

REFERENCES

(1) Chhajed, S.; Schubert, M. F.; Kim, J. K.; Schubert, E. F. *Appl. Phys. Lett.* **2008**, *93*, 251108−251108−3.
(2) An, S. J.; Chae, J. H.; Yi, G.-C.; Park, G. H. *Appl. Phys. Lett.* **2008**, *92*, 121108−121108−3.
(3) Wang, S. J.; Sun, X. W.; Yang, Y.; Huang, H.; Lee, Y. C.; Tan, O. K.; Vayssieres, L. *Nanotechnology* **2006**, *17*, 4995−4998.
(4) Lohmüller, T.; Helgert, M.; Sundermann, M.; Brunner, R.; Spatz, J. P. *Nano Lett.* **2008**, *8*, 1429−1433.
(5) Zhu, G.; Yang, R.; Wang, S.; Wang, Z. L. *Nano Lett.* **2010**, *10*, 3151−3155.
(6) Huang, J.-H.; Chen, C.-Y.; Lai, Y.-F.; Shih, Y.-I.; Lin, Y.-C.; He, J.-H.; Liu, C.-P. *Cryst. Growth Des.* **2010**, *10*, 3297−3301.
(7) Choi, K.; Park, S. H.; Song, Y. M.; Lee, Y. T.; Hwangbo, C. K.; Yang, H.; Lee, H. S. *Adv. Mater.* **2010**, *22*, 3713−3718.
(8) Xu, H.; Lu, N.; Qi, D.; Hao, J.; Gao, L.; Zhang, B.; Chi, L. *Small* **2008**, *4*, 1972−1975.
(9) Du, Y.; He, H.; Jin, Y.; Kong, F.; Guan, H.; Fan, Z. *Appl. Surf. Sci.* **2012**, *258*, 6431−6435.
(10) Yang, Z.-P.; Ci, L.; Bur, J. A.; Lin, S.-Y.; Ajayan, P. M. *Nano Lett.* **2008**, *8*, 446−451.
(11) Joo, W.; Kim, H. J.; Kim, J. K. *Langmuir* **2009**, *26*, 5110−5114.
(12) Yeh, L.-K.; Lai, K.-Y.; Lin, G.-J.; Fu, P.-H.; Chang, H.-C.; Lin, C.-A.; He, J.-H. *Adv. Energy Mater.* **2011**, *1*, 506−510.
(13) Li, H.; Jiang, B.; Schaller, R.; Wu, J.; Jiao, J. *J. Phys. Chem. C* **2010**, *114*, 11375−11380.
(14) Chao, Y.-C.; Chen, C.-Y.; Lin, C.-A.; He, J.-H. *Energy Environ. Sci.* **2011**, *4*, 3436−3441.
(15) Gayen, R. N.; Dalui, S.; Rajaram, A.; Pal, A. K. *Appl. Surf. Sci.* **2009**, *255*, 4902−4906.
(16) Yu, H. K.; Baik, J. M.; Lee, J.-L. *Cryst. Growth Des.* **2011**, *11*, 2438−2443.
(17) Yu, H. K.; Baik, J. M.; Lee, J.-L. *ACS Nano* **2011**, *5*, 8828−8833.
(18) Chao, Y.-C.; Chen, C.-Y.; Lin, C.-A.; Dai, Y.-A.; He, J.-H. *J. Mater. Chem.* **2010**, *20*, 8134−8138.
(19) Yin, Z.; Liu, X.; Wu, Y.; Hao, X.; Xu, X. *Opt. Express.* **2012**, *20*, 1013−1021.
(20) Ghosh, R.; Dutta, M.; Basak, D. *Appl. Phys. Lett.* **2007**, *91*, 073108−073108−3.
(21) Lee, Y.-J.; Ruby, D. S.; Peters, D. W.; McKenzie, B. B.; Hsu, J. W. P. *Nano Lett.* **2008**, *8*, 1501−1505.
(22) Joo, J.; Chow, B. Y.; Prakash, M.; Boyden, E. S.; Jacobson, J. M. *Nat. Mater.* **2011**, *10*, 596−601.
(23) Xu, S.; Lao, C.; Weintraub, B.; Wang, Z. L. *J. Mater. Res.* **2008**, *23*, 2072−2077.
(24) Fang, F.; Zhao, D.; Zhang, J.; Shen, D.; Lu, Y.; Fan, X.; Li, B.; Wang, X. *Mater. Lett.* **2008**, *62*, 1092−1095.
(25) Chen, J. Y.; Sun, K. W. *Sol. Energy Mater. Sol. Cells* **2010**, *94*, 930−934.
(26) Raut, H. K.; Ganesh, V. A.; Nair, A. S.; Ramakrishna, S. *Energy Environ. Sci.* **2011**, *4*, 3779−3804.
(27) Riley, M.; Redo-Sanchez, A.; Karampourniotis, P.; Plawsky, J.; Lu, T.-M. *Nanotechnology* **2012**, *23*, 325301.
(28) Macleod, H. A. *Thin-Film Optical Filters*; Hilger: Bristol, U.K., 1986.